

Development of a new LAr Purity Monitor: Design of the α -Source

Diploma Thesis

Marco Laffranchi, Institute for Particle Physics, ETH Zurich

under the supervision of

Prof. Dr. André Rubbia
Dr. Andreas Badertscher

September 21, 2000

Abstract

The development and construction of a liquid argon (LAr) purity monitor for the ICARUS experiment is described. The monitor is based on a lifetime measurement of electrons in LAr. To determine the lifetime of electrons in LAr, the charge of the ionization electrons produced by an α -source is measured at the beginning and at the end of a drift path of about 10 cm length, together with the drift time. The electrodes producing the drift field are chosen as spheres with a diameter of about 0.5 mm with the Pb^{210} α -source situated on the surface of the cathode. This geometry has the advantage that, on the one hand, the electrons are produced in a high electric field near the surface of the cathode, which suppresses the recombination, and, on the other hand, it produces small drift fields along the drift path to obtain long drift times of the order of ms.

Contents

1	Introduction	2
1.1	The ICARUS Experiment	2
1.2	Overview of Purity Monitor Design	4
2	Design Study for the Purity Monitor	8
2.1	The Electric field	8
2.2	Calculation of the Number of Free Electrons	11
2.2.1	Energy Deposition of α -Particles in LAr	11
2.2.2	Recombination Models	12
2.2.3	Results	14
2.3	Calculation of Drift Velocity and Drift Times	17
3	Setup	24
3.1	Measuring Setup	24
3.2	Preparation of the Spherical Source	24
3.3	Mechanics of the Purity Monitor	26
3.4	Electronics and Data Acquisition	29
4	Measurements	34
4.1	Calibration of the Charge Preamplifier	34
4.2	Measured Charge of the Electron Cloud	37
5	Conclusion	41

Chapter 1

Introduction

1.1 The ICARUS Experiment

The ICARUS (Imaging Cosmic And Rare Underground Signal) experiment [1] will take place at the Gran Sasso National Laboratory near Rome. A novel liquid argon drift chamber was developed as a particle detector. The ICARUS program addresses many fundamental issues:

- the nature of neutrinos, in particular the question of the neutrino mass. This is being investigated in ICARUS both through the study of atmospheric neutrinos and through long baseline studies with the foreseen CERN neutrino beam;
- the stability of the nucleon, which is the only way to access phenomena at the energy scale of Grand Unification. ICARUS will be the first high-resolution imaging study of such a phenomenon;
- the study of solar neutrinos. Even though ICARUS is not optimized to study this kind of events, the issue remains extremely interesting and with a suitable neutron shielding ICARUS can reach a reasonable detection threshold;
- the detection of astrophysical and cosmological neutrinos from supernova.

As a LAr TPC (time projection chamber), ICARUS has the advantage of being operated over a very large sensitive volume, continuously sensitive, self-triggering, able to provide three-dimensional views of ionizing events with particle identification from dE/dx and range measurements. At the same time, the detector acts also as a good homogeneous calorimeter of very fine

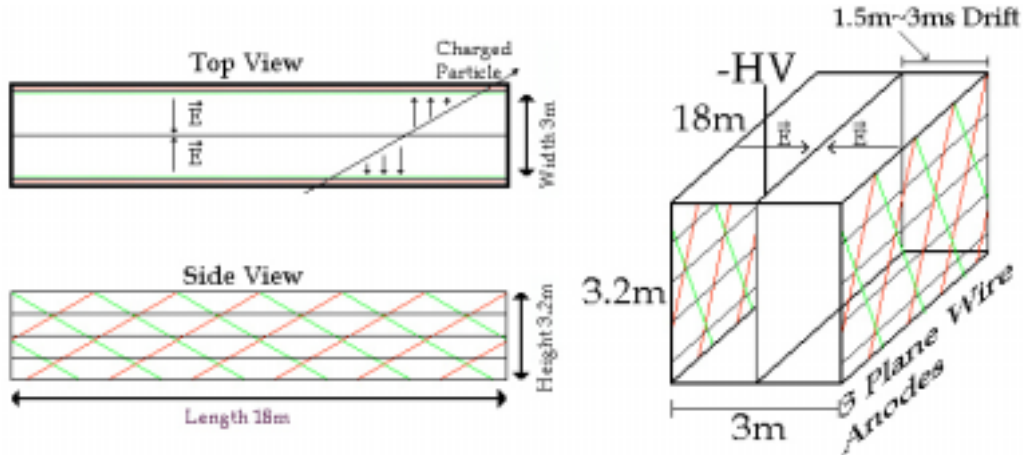


Figure 1.1: Schematic view of a 300t halfmodule of the ICARUS experiment. The drift field is $E=500\text{V}/\text{cm}$ yielding a drift velocity $v_{drift} = 1.5\text{mm}/\mu\text{s}$.

granularity and high accuracy. The ICARUS project requires a sensitive LAr mass of the order of several kilotons, therefore, this type of detector can be considered as an ideal device for a rare event search.

A modular approach was adopted to reach this sensitive mass, with modules as big as possible, but still able to be moved from the construction site to the Gran Sasso Laboratory. Each module of 600t LAr is composed of two sub-modules of 300t each (see picture 1.1), which can be transported by truck.

The first 600t module is being assembled now at Pavia, and is planned to be moved to the Gran Sasso Laboratory next year. It will allow an important first step in the ICARUS scientific program. In fact, this detector has enough mass to investigate the atmospheric and solar neutrinos; while a much larger sensitive mass of thousands of tons is needed to detect astrophysical neutrinos, to achieve the 10^{34} years range in proton decay lifetime and to detect the (oscillating-)neutrinos coming from the long baseline neutrino beam at CERN.

The operating principle of the ICARUS liquid argon TPC is rather simple: any ionizing event (from particle interaction or decay), taking place in a volume of liquid argon, produces ion-electron pairs. A fraction of them will not recombine and will drift parallel to the uniform E-field (applied in opposite directions, see picture 1.1). Only the motion of the much faster electrons induces a current on a number of parallel wire planes located at the end of the sensitive volume. The orientation of the wires of the three planes with respect to the horizontal direction is $+60^\circ$, 0° and -60° and together with

a measurement of the drift time, provide a full 3-D image reconstruction of the event.

The LAr, used as absorber and active detector, was chosen by the following considerations:

1. it is an excellent electric insulator and available at an extremely high purity level;
2. the ionization density is high enough to get measurable pulse heights even for minimum ionizing particles.
3. it is easily available in large quantities because of its high abundance (about 1%) as a natural component of the Earth's atmosphere; it is thus cheaper than other heavy noble gases.

The purity of the LAr is fundamental in order to reach long drift paths in the TPC. Electronegative impurities capture the electrons and hence decrease the charge measured with the wire chambers at the end of the drift. The purity of LAr decreases in time due to outgassing of the dewar walls and detector materials, thus, the LAr has to be circulated through a purification stage and the mean life-time of the drifting electrons has to be monitored continuously, in order to keep the purity at the level necessary for a good operation of the TPC. From the parameters for the 300t module follows that life-times of the order of ms are needed.

1.2 Overview of Purity Monitor Design

For homogeneously distributed impurities we can assume that the capture rate of the free electrons in LAr is constant along the drift. This results in an exponential decay of the number of free electrons with a mean life-time τ :

$$N = N_0 \cdot e^{-\frac{t_{drift}}{\tau}} \quad (1.1)$$

where N_0 , N are the number of electrons at the beginning and at the end of the drift,
 t_{drift} is the drift time,
 τ is the mean life-time of electrons in LAr.

The purity monitor described in the following chapters is based on the life-time measurement using the drift method, which consists of producing free electrons in LAr, measure the initial charge (N_0), drift them for a certain

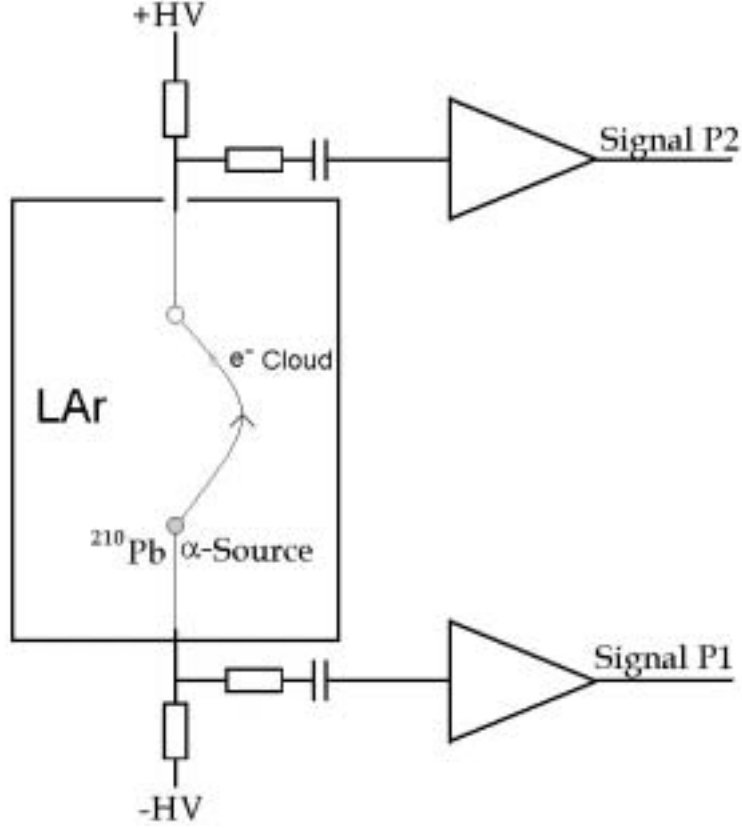


Figure 1.2: Schematic view of the proposed purity monitor.

time (t_{drift}) and measure again the remaining charge (N); the life-time will come out directly from eq. 1.1:

$$\tau = -\frac{t_{drift}}{\ln \frac{N}{N_0}} \quad (1.2)$$

In our case, the electrons are produced by a 3.72 MeV α -particle emitted by the Pb^{210} source, placed on the surface of the spherical platinum cathode (see figure 1.2). The α -particles have a very high ionization density in LAr, which usually leads to a high recombination rate of the electron-ion pairs. The recombination can be reduced by applying a high E-field along the ionization region, but, on the other hand, low E-fields are needed for long drift times. The small range of about $30\mu\text{m}$ of the 3.72 MeV α -particles in LAr has the advantage, that all the electron-ion pairs are concentrated near the surface of the cathode where the E-field is high. Thus a spherical cathode with a diameter of about 0.5 mm will give a sufficiently high E-field in the

ionization region but also very small fields at cm distances.

A β -source would have the disadvantage that the long range β -particles, emitted at all angles, generate a non localized cloud of ionization electrons. This would make it difficult to uniformly collect the charges and would also introduce constraints on the shape of the E-field.

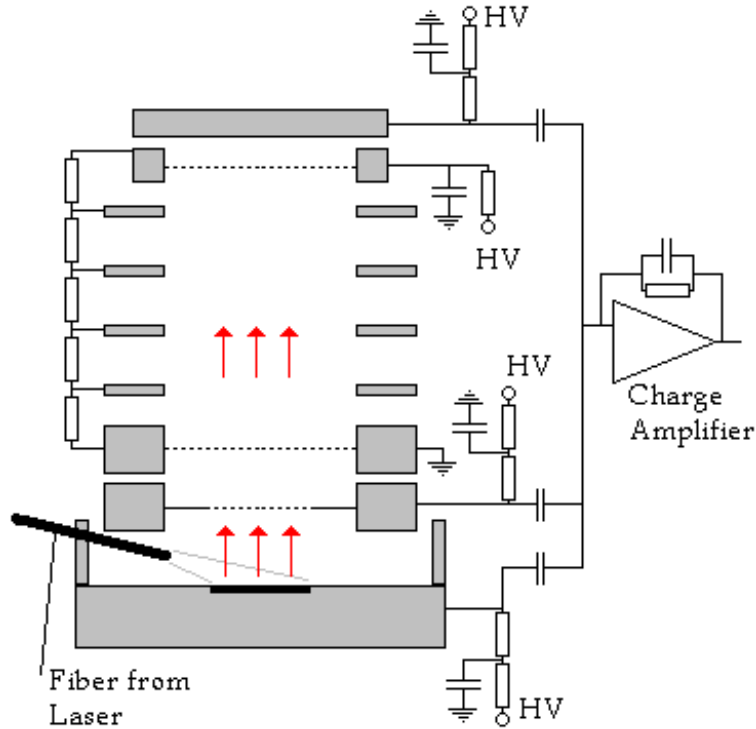


Figure 1.3: LAr purity monitor for the ICARUS experiment, using a laser to produce free electrons.

The purity monitor built by the L'Aquila Group for ICARUS [1] is also based on a life-time measurement (see figure 1.3). The electrons, in this case, are produced on a photocathode by UV light coming from a pulsed xenon lamp (or laser) which is operated outside of the dewar. A disadvantage of this method is that the UV light has to be brought to the cathode through quartz fibers, which is very delicate and could turn out not be stable over a long time period.

Purity monitors used in experiments with a LAr calorimeter, such as e.g. Atlas, D0 and H1 measure the charge of the electrons in an ionization chamber with a plane geometry. This method, contrary to the drift method, does not give a direct measurement of the mean life-time but a relative measure of

the LAr purity [2]. These purity monitors use radioactive alpha (see figures 1.4) or beta sources or a laser (photoeffect) to produce free electrons. Given the lack of a long drift region, the precision reached with such methods is not good enough for mean life-times $> 100\mu s$, and ICARUS TPC will need $\tau > 3ms$.

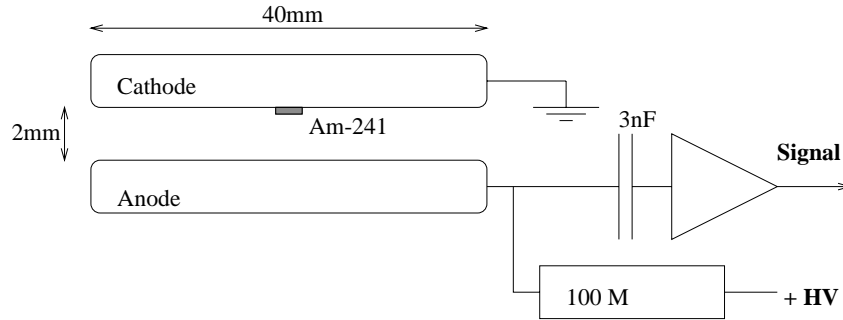


Figure 1.4: Purity monitor with an α -source for the LAr calorimeter of the ATLAS experiment[2].

Chapter 2

Design Study for the Purity Monitor

To study the feasibility of a purity monitor, based on the new source, the expected number of electrons produced by the Pb^{210} -source was calculated, taking into account the energy deposition of the α -particles in LAr and the recombination of the electrons with the positive ions as a function of the electric field strength.

The electrons were then traced along the field lines of the dipole configuration to the anode to calculate the drift time for different distances between the cathode (source) and the anode and for different high voltages. The diffusion of the electron cloud in LAr is also investigated.

2.1 The Electric field

The two spherical electrodes produce a dipole field (see figure 2.1), which is easily described analytically by a superposition of Coulomb fields (see eq. 2.1). To limit the dipole field to a given diameter, field shaping electrodes will be necessary (see figure 2.14).

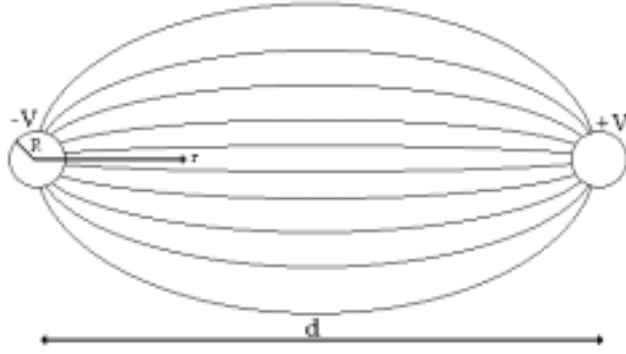


Figure 2.1: Dipole field produced by two spherical electrodes placed at voltages of $+V$ and $-V$.

For the cathode position at $\vec{r} = 0$ and the anode at $\vec{r} = \vec{d}$, the \vec{E} -field is given by:

$$\vec{E} = \frac{V \cdot R}{r^2} \frac{\vec{r}}{|\vec{r}|} + \frac{V \cdot R}{(\vec{r} - \vec{d})^2} \frac{(\vec{r} - \vec{d})}{|(\vec{r} - \vec{d})|} \quad (2.1)$$

- where \vec{E} is the E-field vector.
 V High voltage applied to the electrodes. The potential difference between the electrodes is $2V$.
 R Radius of the electrodes.
 \vec{r} Position relative to the source (cathode).
 \vec{d} Position of the anode with respect to the cathode.

Such a field is high near the surface of the source ($r=R$) and low in the middle of the drift region ($r \approx d/2$).

Close to the source the E-field is well approximated by a single Coulomb field, i.e. (eq. 2.1 in the limit $\lim |\vec{r}| \rightarrow 0$)

$$|\vec{E}| = \frac{V \cdot R}{r^2} \quad (2.2)$$

The E-field is linearly dependent on the applied high voltage. For a given HV ($\pm V$), a smaller source radius will produce a higher field around the source and, at the same time, a smaller field in the drift space (see figure 2.2). Reducing the distance between the two electrodes will increase the field in the central region (see figure 2.3). Note, that with the spherical electrodes a very low drift field in the drift space of the order of a few V/cm can easily be reached. For example for $V=4\text{kV}$, $R=0.25\text{mm}$ and $d=30\text{cm}$ the field at

the surface of the cathode is 160kV/cm and only 1V/cm in the middle of the drift region (see figure 2.3).

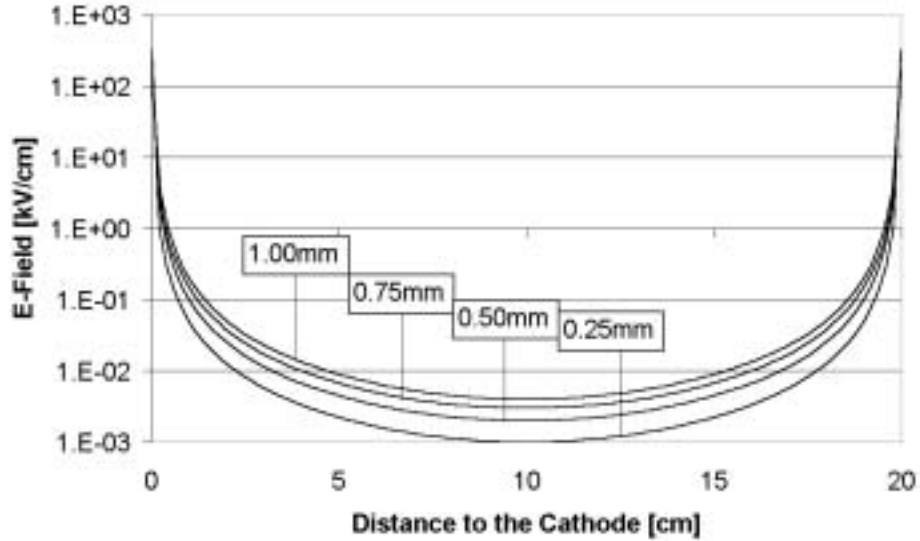


Figure 2.2: E-field on the axis, calculated with eq. 2.1 with $d=20\text{cm}$ and $V=4\text{kV}$. The parameters shown are the values of R .

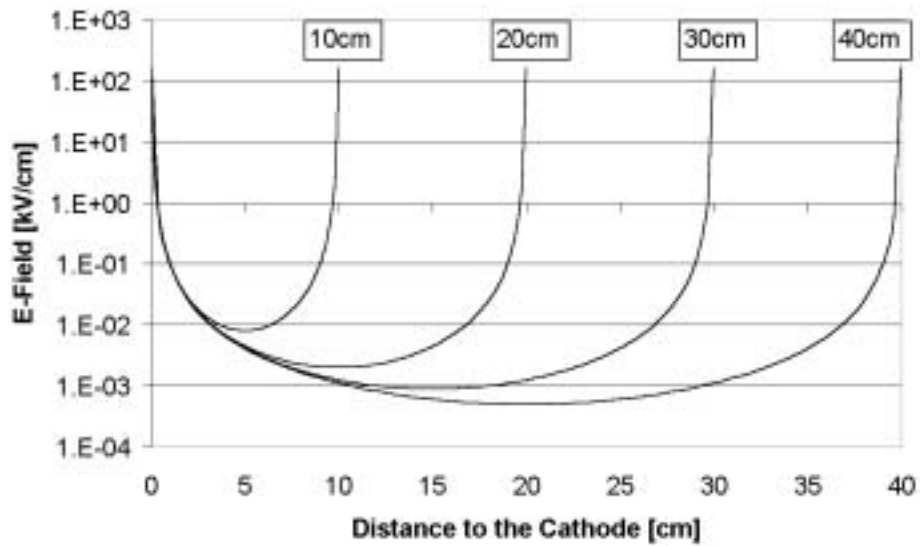


Figure 2.3: E-field on the axis, calculated with eq. 2.1 with $R=0.5\text{mm}$ and $V=4\text{kV}$. The parameters shown are the values of d .

2.2 Calculation of the Number of Free Electrons

2.2.1 Energy Deposition of α -Particles in LAr

The energy loss dE/dx (in MeV/cm) of the α -particle in the LAr is given by the well known Bethe-Bloch formula[3]:

$$\frac{dE}{dx} = 0.1535 \cdot \rho \frac{Z}{A} \cdot \frac{z^2}{\beta^2} \cdot \left[2 \ln \left[2 \cdot 511000 \frac{\gamma^4 \beta^2}{I_0} \right] - 2 \cdot [\beta]^2 \right] \quad (2.3)$$

where	$m=3728.4 \text{ MeV}/c^2$	Mass of the α -particle,
	$z=2$	Charge of α particle (in units of e),
	$\rho = 1.4 \text{ g/cm}^3$	Density of LAr,
	$Z=18$	Atomic number of Ar,
	$A=39.948 \text{ g/mol}$	Molar mass of Ar,
	$I_0 = 210 \text{ eV}$	Mean ionization potential of Ar,
	$T[\text{MeV}]$	Kinetic energy of the particle.
	γ	Lorentz factor of the particle
	β	Velocity of the particle in units of c

With the previous formula, one can calculate the Bragg curve of the α particle. The resulting ionized electron density in Argon is shown in Figure 2.4 as a function of the path length. We observe that the ionization of the α is as expected very large (about 700 times ionisation density of a MIP) and

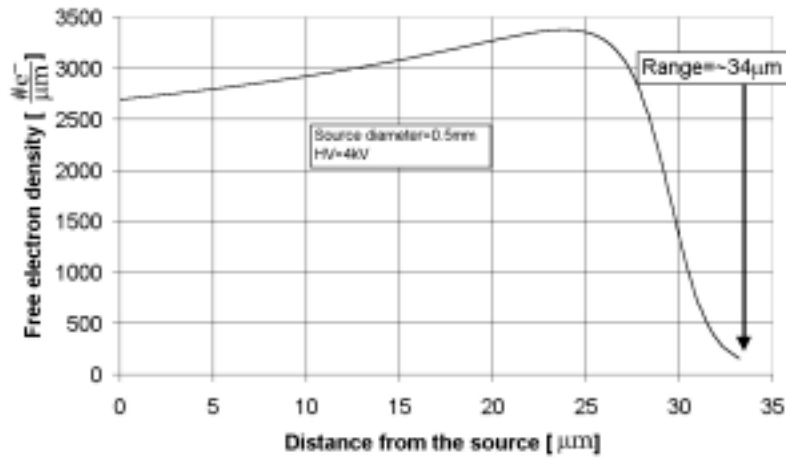


Figure 2.4: Bragg curve of a 3.72MeV α -particle.

this has the effect that the range of the α will be very short. In particular, for the 3.72MeV α that we consider, we obtain a range of about 30 microns. The Bragg curve does not exhibit the usual strong "peak" at the end of the range because the quenching of the ionization electrons has already been included in the curve.

2.2.2 Recombination Models

The Birks Model [1][p.50] gives a semi-empirical formula for the recombination of electron-ion pairs at a given E-field, which takes into account the ionization density of the particle. The formula has only one parameter k_1 , which is strongly dependent on the E-field (see figure 2.6). The electron density after recombination is given by:

$$\frac{dN}{dx} = \frac{\frac{dE}{dx} \cdot \frac{1}{w}}{1 + k_1(|\vec{E}|) \frac{dE}{dx} \cdot \frac{1}{\rho}} \quad (2.4)$$

where $w = 23.6eV$ is the mean energy needed to produce an e^- -ion pair,
 $\frac{dE}{dx}$ is the energy deposited by the particle calculated
with the Bethe-Bloch formula (see section 2.2.1),
 $\rho = 1.4g/cm^3$ is the density of the LAr,
 $|\vec{E}|$ is the E-field in the recombination region,
 $k_1(|\vec{E}|)$ is the Birks factor.

The value of the Birks factor for LAr is only given for a field of $E=500V/cm$ in [1]^(p.50)

$$k_1(500V/cm) = 0.1075g \cdot MeV^{-1} \cdot cm^{-2} \quad (2.5)$$

In order to calculate the recombination for different high voltages and for the varying field along the range of the α -particles, the Birks factor has to be known as a function of the E-field. We decide to use the Box Model [4] to estimate the values of the Birks factor at different E-fields.

In the Box Model, the ion-electron pairs are considered as isolated and, at the beginning, the distribution is uniform in a box of certain dimensions. With these assumptions the ratio between the number of electrons before and after the recombination can be described by a formula containing one parameter C. The ratio of the number of electrons with and without recombination is expressed as:

$$\frac{N}{N_0} = \frac{|\vec{E}|}{C} \ln\left(1 + \frac{C}{|\vec{E}|}\right) \quad (2.6)$$

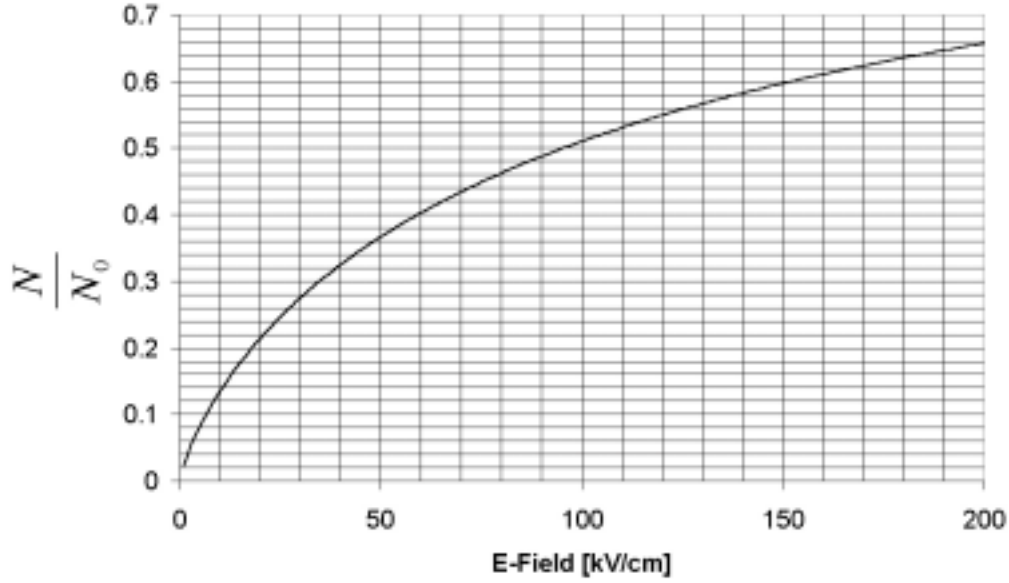


Figure 2.5: Ratio of electrons with and without recombination as a function of the E-field predicted by the Box Model. The curve is calculated for 3.72MeV α -particles in LAr.

Were $|\vec{E}|$ is the homogeneous E-field in the recombination region. The parameter C depends on the type of radioactive source and the ionized medium (i.e. the ionization density distribution), but it does not depend on the E-field. For our ${}_{82}\text{Pb}^{210}$ -source, emitting 3.72MeV α -particles, it comes out as $C=239.9$ (see next paragraph). For an ${}_{95}\text{Am}^{241}$ -source with 5.49MeV α -particles, $C=243.0$.

The determination of the C factor for a Pb^{210} α -source in LAr is made as follows: integrating numerically the Birks formula (2.4) with the known Birks factor at $E=500\text{V/cm}$ yields the number of free electrons N produced by a 3.72 MeV α -particle in LAr for a homogeneous field of $E=500\text{V/cm}$; from the integration with $k_1=0$ the number of electrons N_0 without recombination is obtained. Introducing the ratio $\frac{N}{N_0}$ and $E=500\text{V/cm}$ into eq. 2.6 and solving it numerically, we obtain the E-field independent constant $C=239.9$. With this C factor for LAr and 3.72MeV α -particles, it is possible to calculate the Birks factor for all E-field. The calculational procedure was to choose a value for the Birks factor k_1 and calculate the ratio $\frac{N}{N_0}$ (by integration of eq. 2.4). With this ratio and the known C factor of the Box Model, one obtains the E-field corresponding to this specific value of the Birks factor from eq. 2.6.

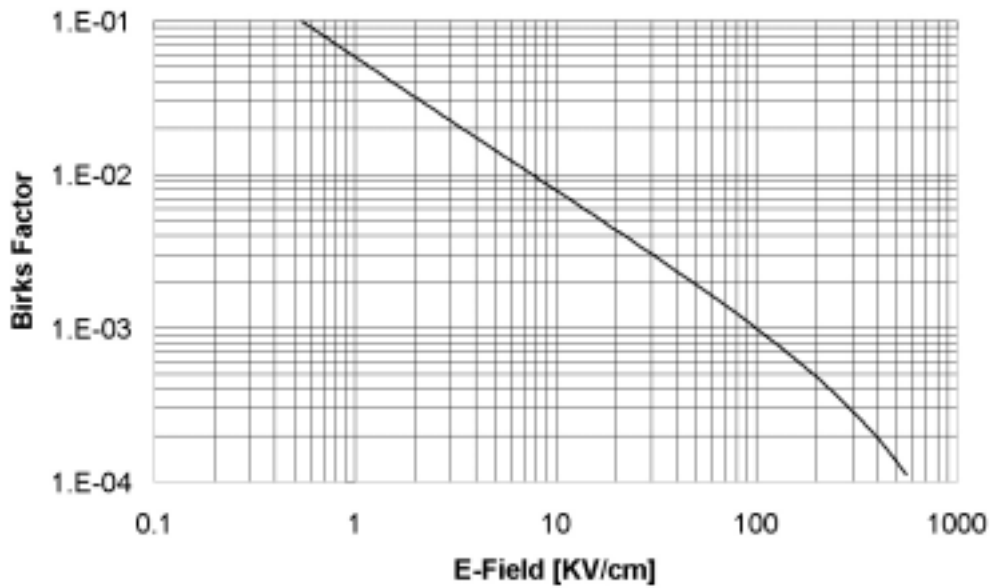


Figure 2.6: Estimated Birks factor k_1 as a function of the E-field.

2.2.3 Results

Figure 2.6 shows the calculated Birks factor dependence on the E-field. At a low E-field the Birks factor is big, this corresponds to a higher recombination rate, which is explicitly shown in figure 2.7, where the electron density distributions is plotted along the range of the α -particle with and without recombination. Both curves were calculated for a spherical source with 0.5mm diameter at 4kV.

The next plots (figure 2.8 and 2.9) show the calculated number of electrons as a function of the high voltage and as a function of the source diameter.

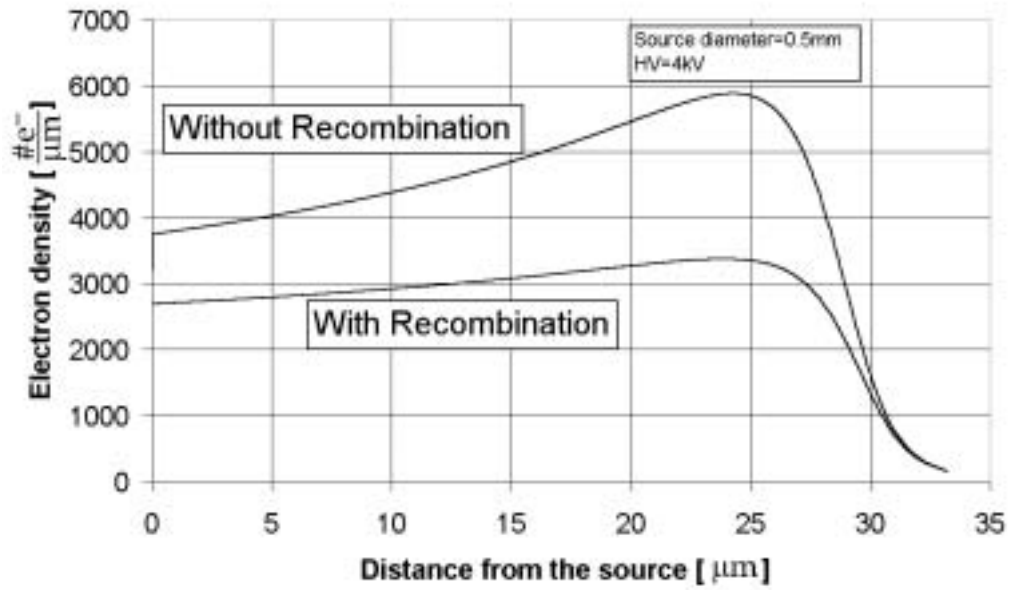


Figure 2.7: Electron density distribution of a 3.72MeV α -particle in LAr with and without e^- -ion recombination. The electrode diameter is 0.5mm and the HV is 4kV.

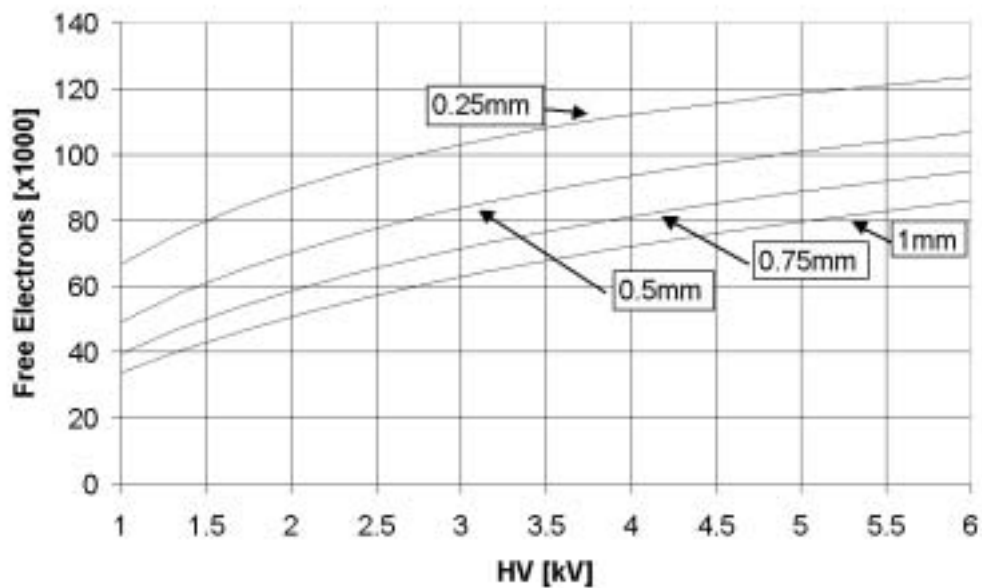


Figure 2.8: Number of free electrons produced by an α -particle in LAr as a function of the HV applied to the electrodes. The curve parameters indicate the diameter of the spherical source.

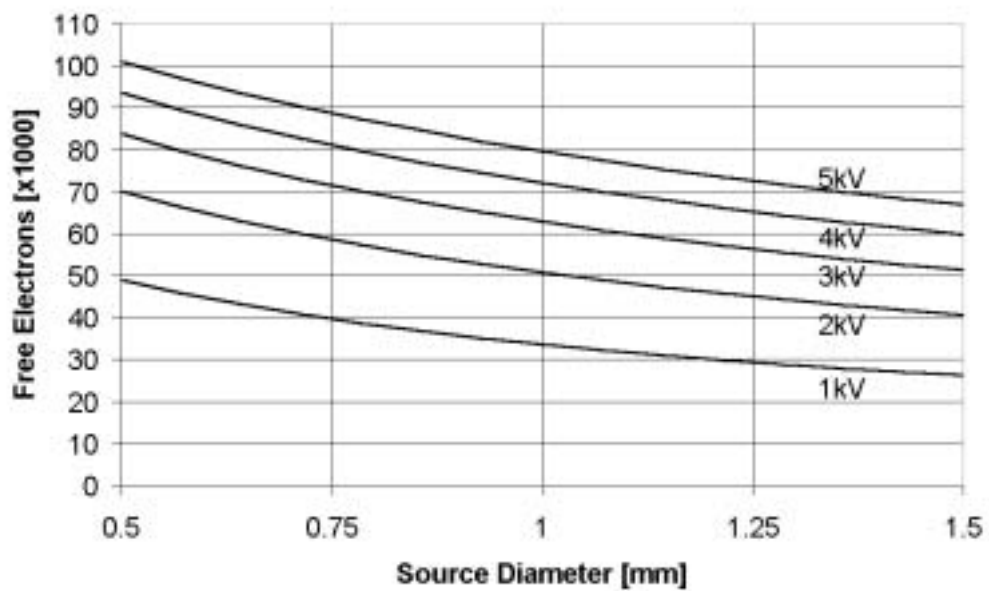


Figure 2.9: Number of free electrons produced by an α -particle in LAr as a function of the diameter of the electrodes. The curve parameters indicate the applied HV.

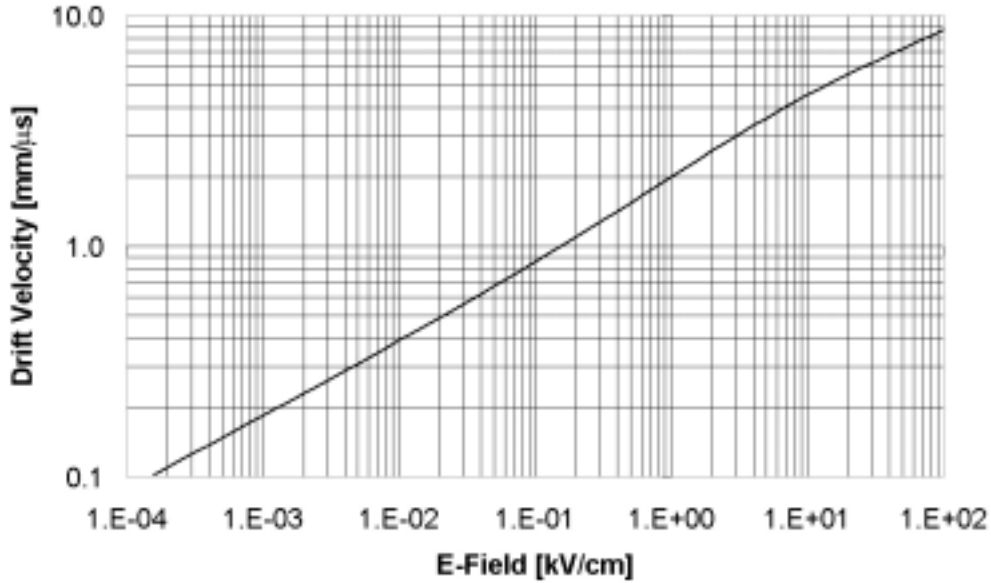


Figure 2.10: Dependence of the drift velocity on the E-field at $T \simeq 90\text{K}$, obtained from eq. 2.7.

2.3 Calculation of Drift Velocity and Drift Times

In this section we calculate the drift time of electrons in LAr as a function of

- the HV applied to the electrodes
- the diameter of the electrodes
- the distance between the electrodes
- the angle α , which determines the starting point of the α (see figure 2.14).

The drift time t_{drift} (see eq. 2.7), i.e. the time it takes the electrons to drift from the source to the anode, should be comparable to the mean life-time for a precise life-time measurement.

For a given HV and geometry (diameter and distance of electrodes) the E-field is fixed and the drift time of the electrons can be calculated knowing the drift velocity of electrons in LAr as a function of E-field [5] (see figure 2.10):

$$v_d \cong P_3 |\vec{E}| \ln \left(1 + \frac{P_4}{|\vec{E}|} \right) + P_5 |\vec{E}|^{P_6} \quad (2.7)$$

where v_d the electron drift velocity at a given E-field
 $|\vec{E}|$ the E-field
 P_3 $0.141 \left(\frac{kV}{cm} \right)^{-1}$
 P_4 $12.4 \left(\frac{kV}{cm} \right)$
 P_5 $1.627 \left(\frac{kV}{cm} \right)^{-P_6}$
 P_6 0.317

Note, that the expression 2.7 with the parameters $P_{3,4,5,6}$ was fitted to data at E-field values of a few kV/cm, while for our case the drift field at the center of the drift region is only a few V/cm. It remains to be checked, whether this expression and the parameter values are valid at such small fields.

The electrons were tracked along the dipole E-field lines through LAr with the help of a Maple computer program. The time step for the tracking was chosen as $0.5\mu s$. The electron cloud is considered here as point-like, starting at the surface of the source. The effect of the diffusion on the time spread of an electron cloud is considered later.

Fig. 2.11 shows the drift time as a function of the HV for different distances between the electrodes. The diameter of the electrodes is 0.5mm and the the HV is $+V$ for the anode and $-V$ for the cathode. Here the electrons drift on the straight line between the electrodes, i.e. it is the minimal drift time. Figures 2.12 and 2.13 show the drift time as a function of the electrode diameter and as a function of the distance between the electrodes. For comparison, we show an hypothetical linear dependence between drift time and drift length. Such a relation would be obtained in the case of a constant electric drift field. We therefore see the advantage of the E-field distribution. For example, for a drift length of 40 cm and a high-voltage of 4kV, we would get a constant field dipole configuration, such drift length and high voltage results in a longer drift time of about 1800 microseconds, i.e. more than a factor two longer.

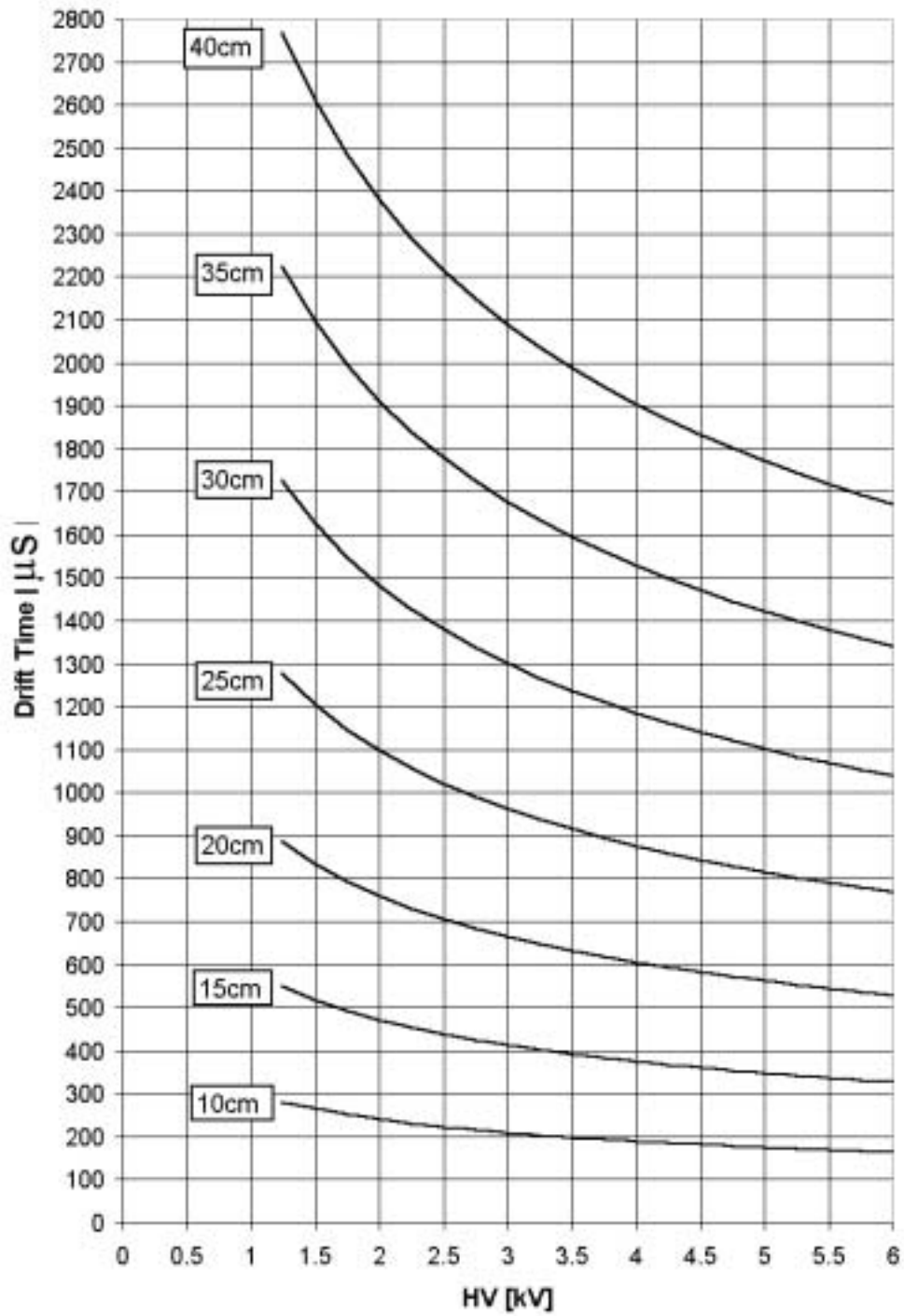


Figure 2.11: Electron drift time as a function of the HV. The curve parameter is the distance between anode and cathode. The diameter of the electrodes is 0.5mm.

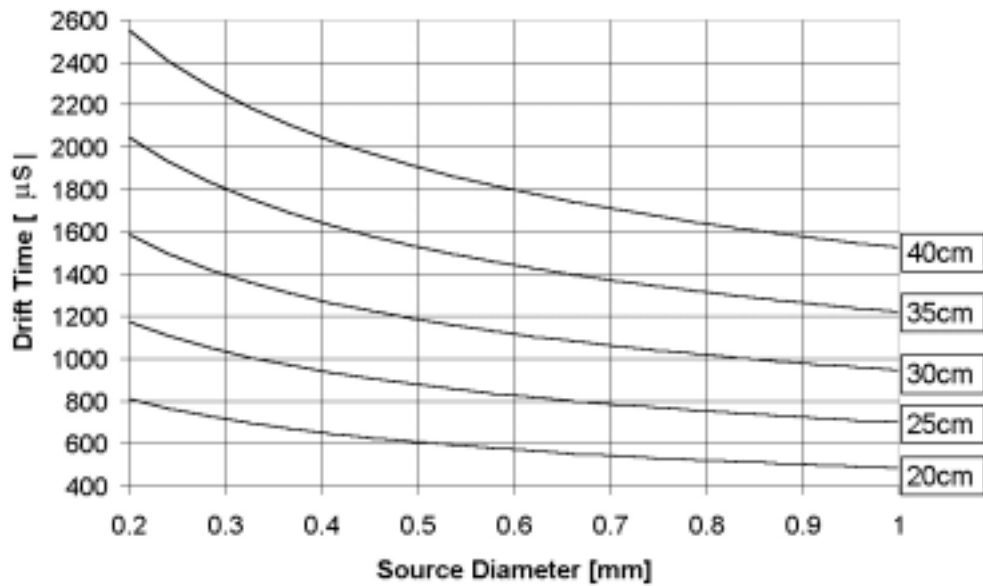


Figure 2.12: Electron drift time as a function of the source diameter. The HV applied is $\pm 4\text{kV}$ and the curve parameter is the distance between the electrodes

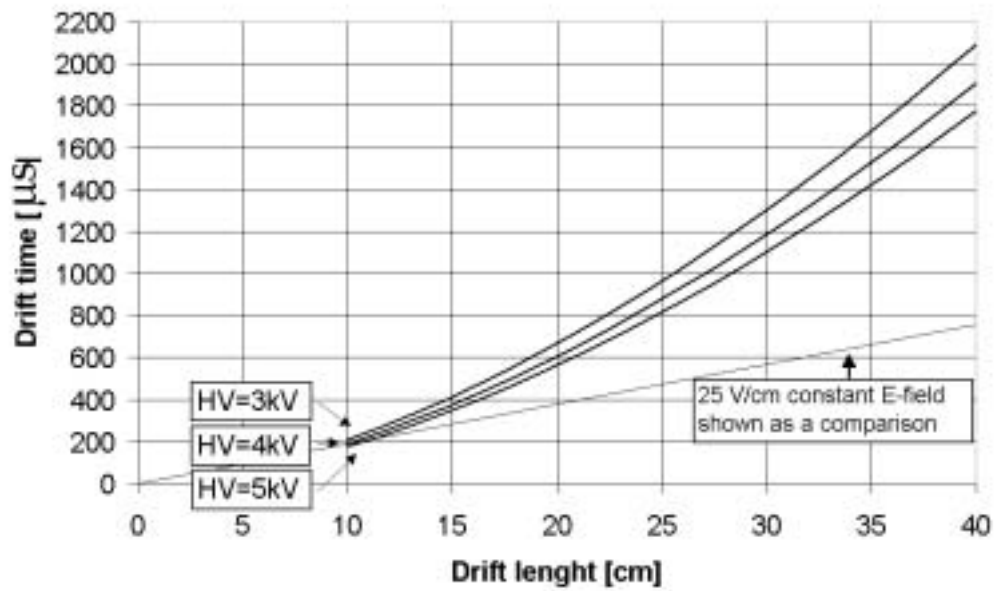


Figure 2.13: Electron drift time as a function of the distance between the electrodes. The diameter of the electrodes is 0.5mm . The curve parameter is the HV.

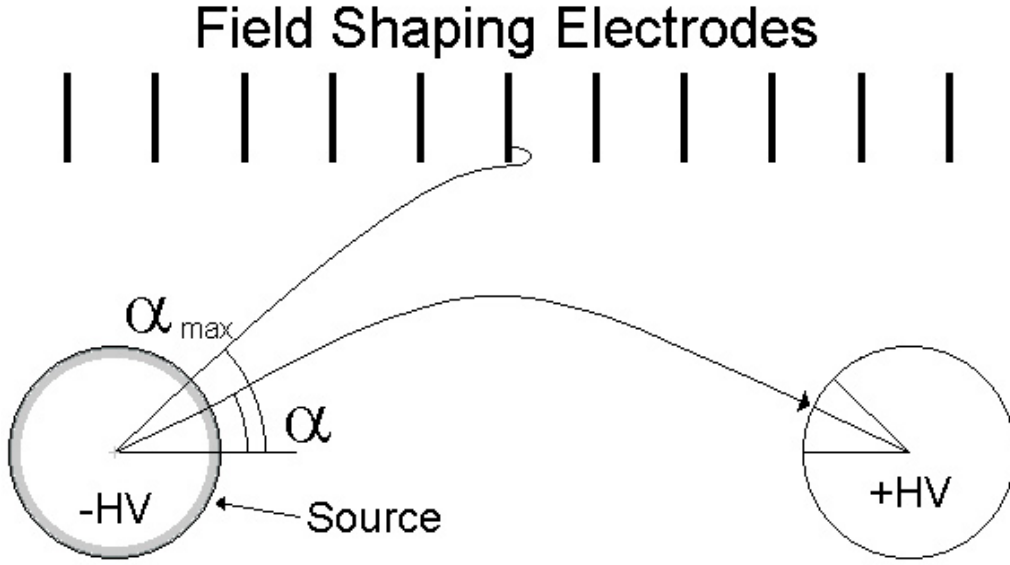


Figure 2.14: Definition of the angles α and α_{max} .

Limiting the dipole field with field shaping electrodes to a certain diameter, implies a cut on the polar angle, α_{max} (see figure 2.14), beyond which the electron cloud can not reach the anode.

Only particles coming from the region on the surface of the source limited by the maximal starting angle α_{max} are seen on the anode. The angle α_{max} is given by:

$$\alpha_{max} \simeq 31.4^\circ \cdot \frac{D_{chamber}}{l} \quad (2.8)$$

where α_{max} is given in degrees, $D_{chamber}$ is the diameter of the purity monitor, l is the distance between the source and the anode. Since the E-field is not homogeneous, particles starting from different points on the surface of the source, have different drift paths and thus different drift times (see figure 2.15).

The diffusion ($\sqrt{2Dt}$) in LAr is very small (diffusion coefficient $D \simeq 5\text{cm}^2/\text{s}$) compared to the gas, however the long drift time and the inhomogeneous E-field have a non negligible influence on the drift time (see figures 2.16 and 2.17). For these calculations, the electrons start at the same point on the surface of the source. Plotted are the 1σ -contours of the Gaussian distribution of the electrons with equal drift times.

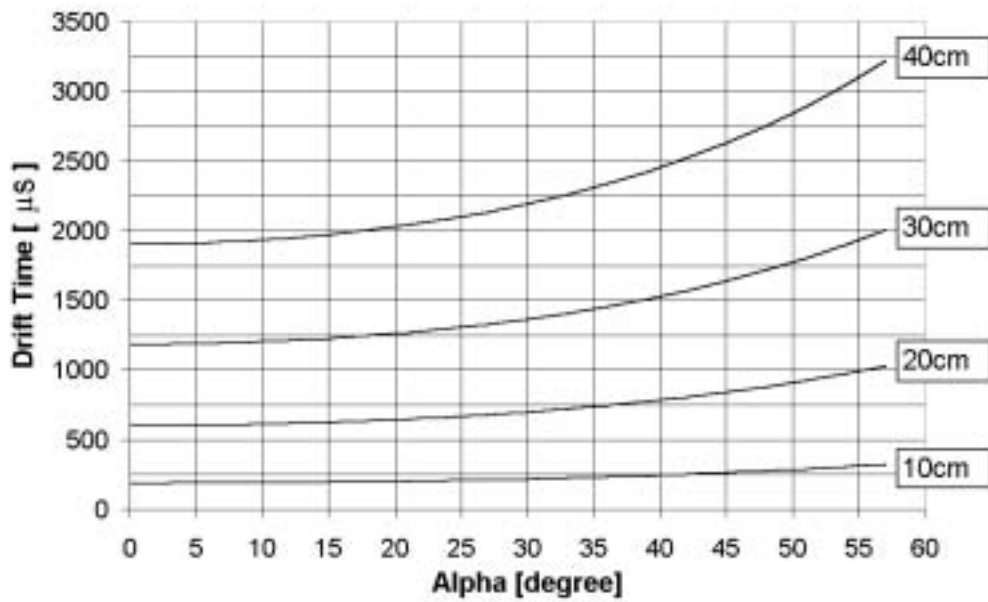


Figure 2.15: Electron drift time as a function of the starting point of the electrons on the surface of the source (determined by the angle α , defined in figure 2.14). The curve parameters are the distance between the anode and the cathode. The HV is $\pm 4kV$.

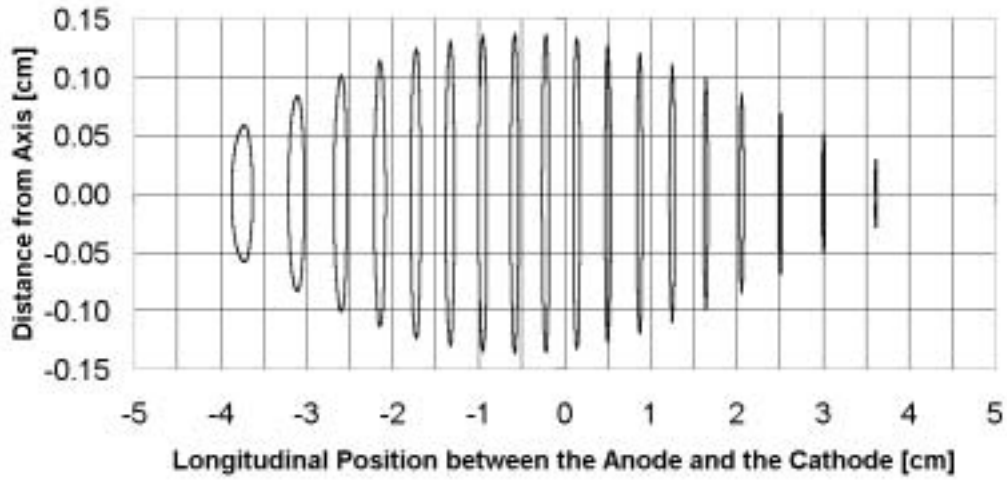


Figure 2.16: Effect of the diffusion of the electron cloud. The cathode with the source is at +5cm longitudinal position and the anode at -5cm. The 1σ -contour of electrons with equal drift times are plotted in intervals of $10\mu s$. The HV is $\pm 4kV$. The starting point of the electrons is at the angle $\alpha = 0^\circ$.

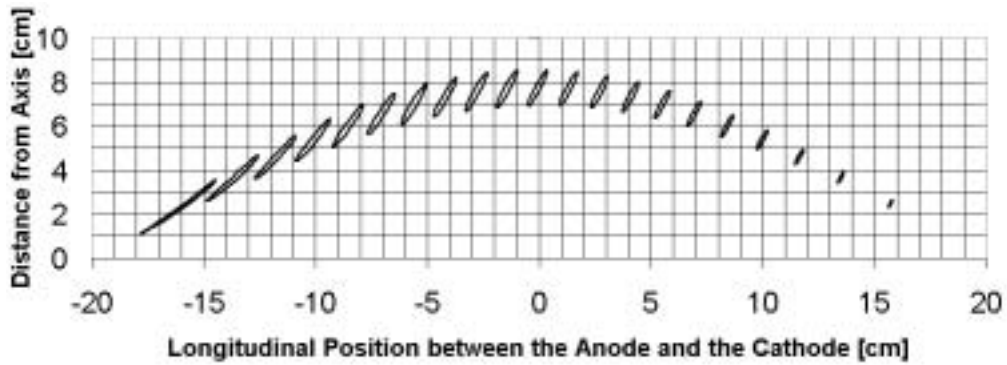


Figure 2.17: Same as previous figure, but for $\alpha = 30^\circ$, a total drift space of 40 cm, plotted in intervals of $100\mu s$.

Chapter 3

Setup

The purity monitor built for the measurements presented in chapter 4 is described. Section 3.4 also contains a proposal for the electronics and data acquisition for a future life-time measurement.

3.1 Measuring Setup

The measurements were made during July 2000. A schematic layout of the measuring setup is shown in fig. 3.1

A commercial open glass dewar was used as cryostat for the purity monitor. To reduce the admixture of oxygen from the air to the LAr, the dewar was covered with plastic foils. The LAr used for the measurements was filled into our storage dewar (Ranger 180 from Air Liquide) at Garbagas, Ruemlang, as type Argon 46 (99.996%), i.e. a technical grade argon without any extra purification. With this setup the measured pulse height from the source was quite stable for many hours (see chapter 4).

3.2 Preparation of the Spherical Source

The spherical α -source with a diameter of about 0.5 mm and an activity of about 10 Bq had to be developed because it is not commercially available. It consists of a thin Pt wire, from which a (roughly) spherical drop was melted at one end in a butane flame. On this Pt drop a thin layer of lead, containing the α -emitter ${}_{82}\text{Pb}^{210}$ (see table below [6] and [7]), was electrolytically applied at the radiochemistry department of PSI, Villigen, Switzerland.

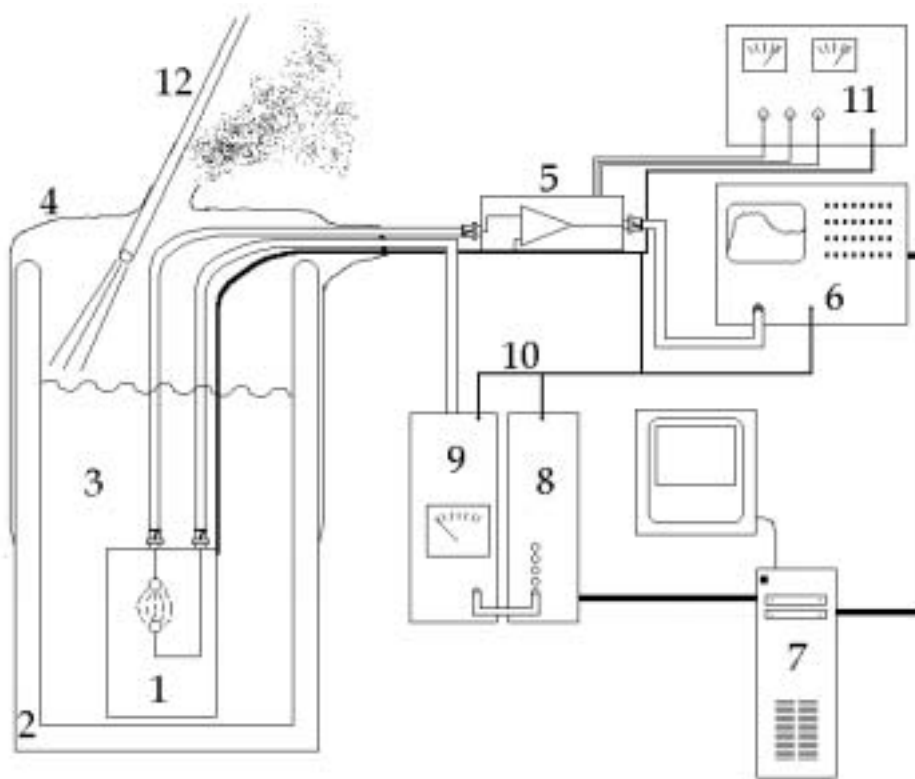


Figure 3.1: Layout of the experiment. 1: purity monitor 2: 10l dewar 3: LAr 4: plastic cover 5: preamplifier 6: storage oscilloscope 7: computer 8: D/A converter for the automatic HV setting 9: HV power supply 10: grounding wire 11: power supply for the preamplifier 12: transfer line to fill the dewar (removed and hole closed after the filling).

Isotope	Life-time	Modes of decay	Decay energy [MeV]	Particle energy [MeV]	Particle intensities
${}_{82}\text{Pb}^{210}$	21y	β	0.061	0.015	0.81
		α	3.72	0.061	0.19
				3.72	1.7×10^{-8}
		γ		~ 0.0465	together with β

The two metals, platinum and lead, were chosen because lead forms a good metallic bond with platinum [8].

The Pt wire used to melt the drops had a diameter of $76\mu\text{m}$. The diameter of the resulting drop depends on the amount of platinum melted, i.e. it can easily be controlled by the time the wire is kept in the flame. Many source holders were produced with this method with diameters in the range of 0.3 to 1.1 mm. Smaller drop diameters would be possible if melted from a wire with a smaller diameter. The source used for the measurements presented in chapter 4 had a diameter of 0.5mm.

The lead source, from which a small activity was put on the Pt holder, was purchased from AEA Technology GmbH, D-38110 Braunschweig, Germany. The lead with a total activity of 20kBq from Pb^{210} was dissolved in 5ml of a 1.2 molar HNO_3 -solution. Higher concentrations of Pb_{210} are available to produce sources of a higher activity. For the electrolysis the HNO_3 -solution was first dried out and the resulting Pb salt was then dissolved in 2ml 1 molar acetic acid and 1 molar NH_4 -acetate solution. The drop of the Pt source holder was then exposed to an electrolysis for 3-4 hours with a current of $I=4\text{mA}$ [8].

3.3 Mechanics of the Purity Monitor

Based on the calculations described in chapter 2, a purity monitor was built with the dimensions as shown in figure 3.4. The distance between the electrodes can be varied between 0-12cm. For the long distances between the electrodes, the Macor rods (a type of ceramic, used as holders) have slits to install cylindrical field shaping electrodes; no field shaping electrodes are drawn in figure 3.4. As a shielding against electromagnetic noise from the environment, the whole monitor is mounted in a stainless steel cylinder, which is covered at the bottom and at the top. The covers have holes at the bottom, to let the LAr flow in, and at the top, to let bubbles escape. On the top cover the signal and HV connectors are mounted.

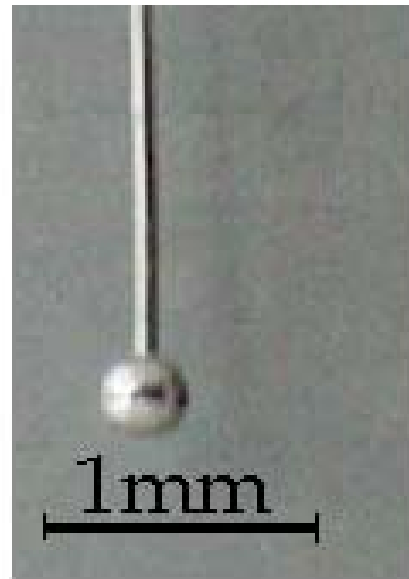


Figure 3.2: Photo of the platinum anode.

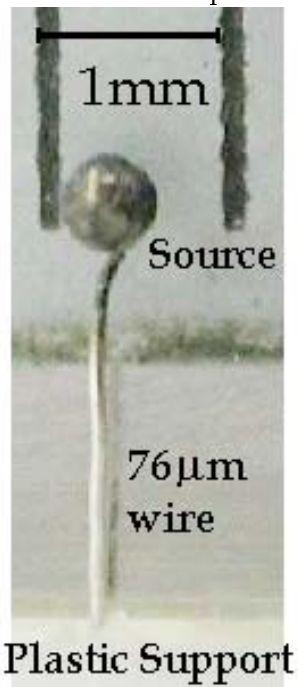


Figure 3.3: Photo of the Pb^{210} source with 0.5mm diameter.

The materials used for the monitor should have good properties at the LAr temperature (87.5K), especially, they should be easy to clean and not outgas too much, in order not to pollute the liquid argon. The insulating parts holding the electrodes are made of Dehoplast [9].

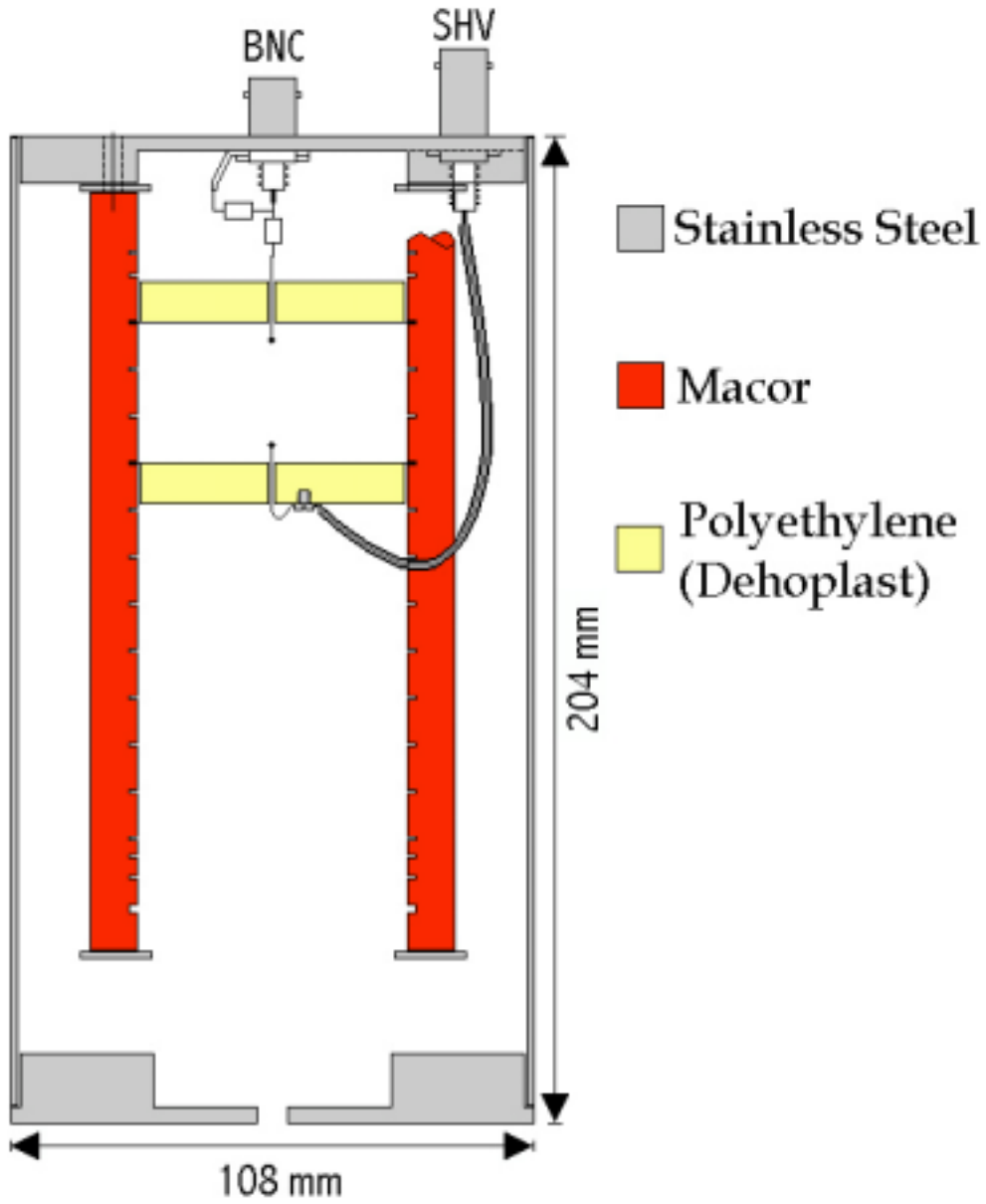


Figure 3.4: Schematic view of the purity monitor.

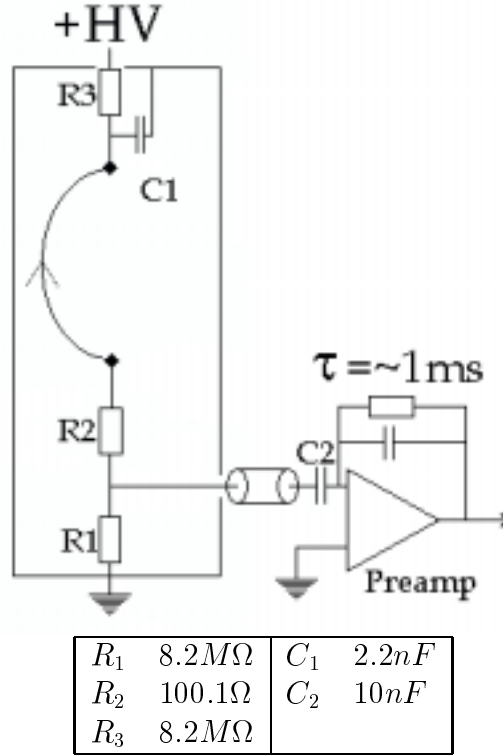


Figure 3.5: Electronics scheme for the measurement of the number of electrons produced by an α -particle in LAr.

3.4 Electronics and Data Acquisition

In this section the electronics used to measure the electron pulses from the source and the data acquisition method are described. At the end of the section, a proposal is made for the electronics to measure the pulses from anode and cathode, together with the drift time, for a life-time measurement.

The electronics scheme used to test the new source is shown in figure 3.5. The preamplifier is of the type developed for the LAr drift chambers of the ICARUS experiment [10] and had a sensitivity of $0.92 \frac{mV}{10ke^-}$ (see section 4.1).

The schematic layout of the experiment is shown in fig. 3.6. The preamplifier is operated outside the LAr dewar at room temperature. The cathode with the source is coupled to the preamplifier through a capacitor and a small resistor protecting the preamplifier. The coaxial signal cable (RG178B/U) connecting the purity monitor with the preamplifier was 1.5m long. The output of the preamplifier was fed into a digital storage oscilloscope (Tektronix

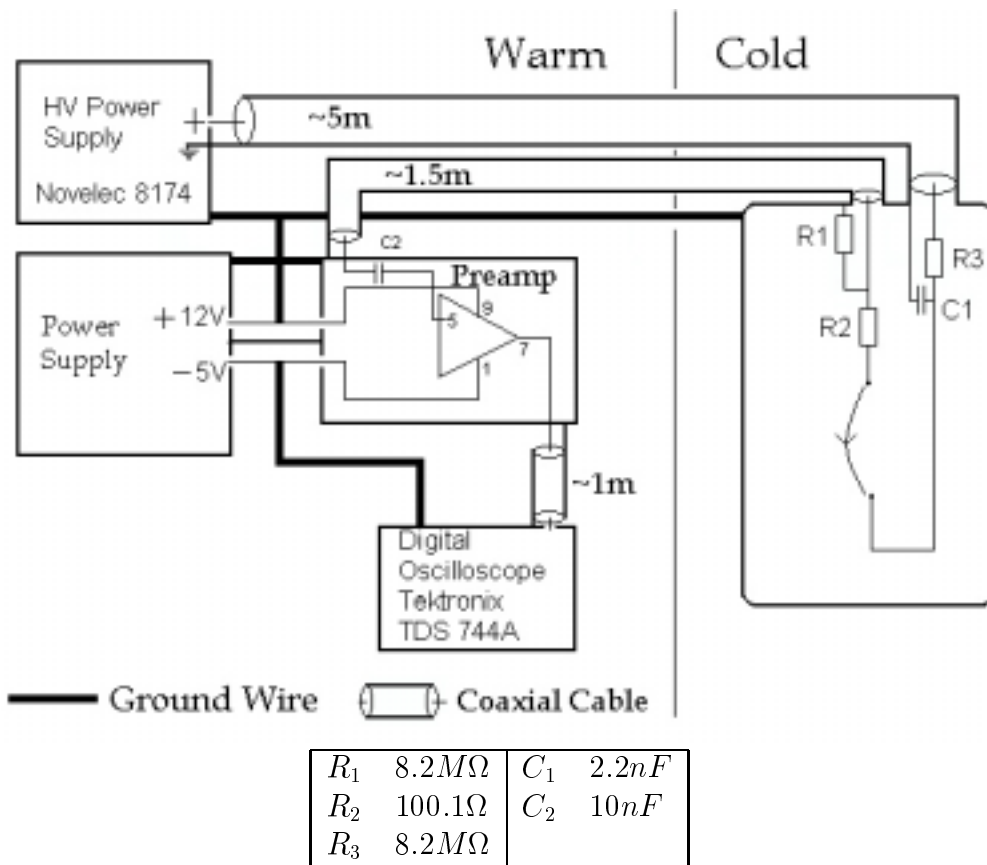


Figure 3.6: Electronics and data acquisition scheme for the measurement of the ionization electrons produced by the α -particles.

TDS744A), which was read out by a PC through the GPIB port. The data were collected with a LabView program running under Windows95.

The trigger set at the oscilloscope was defined to detect a fast raising slope: the lower and the upper threshold (0 and -0.7 mV) had to be crossed by the signal within a time interval of 100ns. This trigger suppressed the low frequency noise very effectively.

Figures 3.7 and 3.8 show the leading edge and the total pulse shape measured with the source. The pulses were superimposed on low frequency noise ($\approx 100Hz$) with an amplitude of about 20mV. The trigger selected pulses around the ground level (0mV), hence, it strongly reduced the measured rate compared to the activity of the source. The pulse height, used to build the spectra presented in chapter 4, was obtained from the sum of the signal levels over 150 channels before and after the signal edge (Σ_1, Σ_2), as shown in figure 3.7.

$$\text{Pulse height} \equiv \frac{\Sigma_1 - \Sigma_2}{150} \quad (3.1)$$

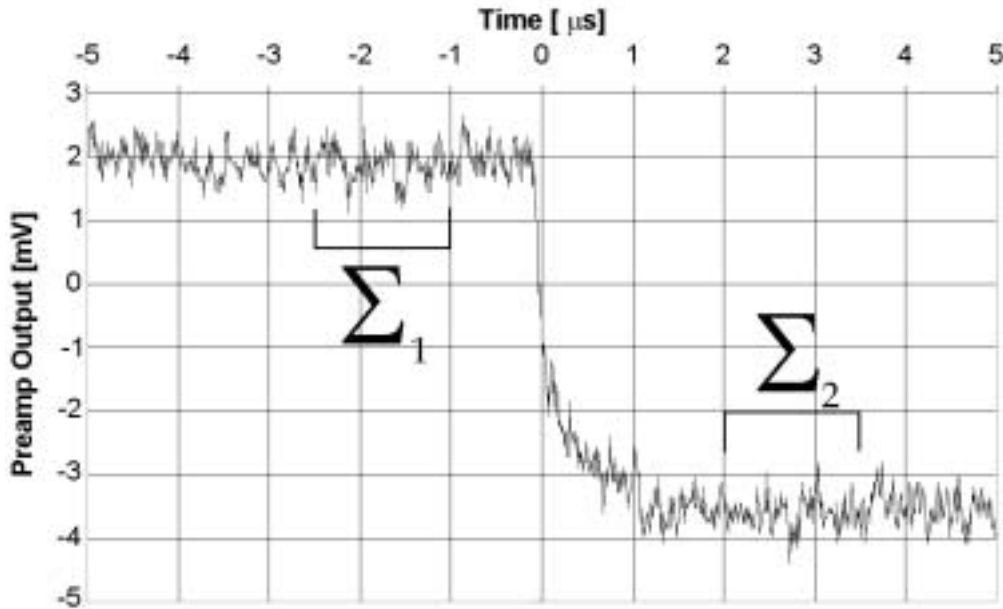


Figure 3.7: Leading edge of a pulse measured with the source. The signal is averaged over Σ_1 and Σ_2 to define the pulse height (see text).

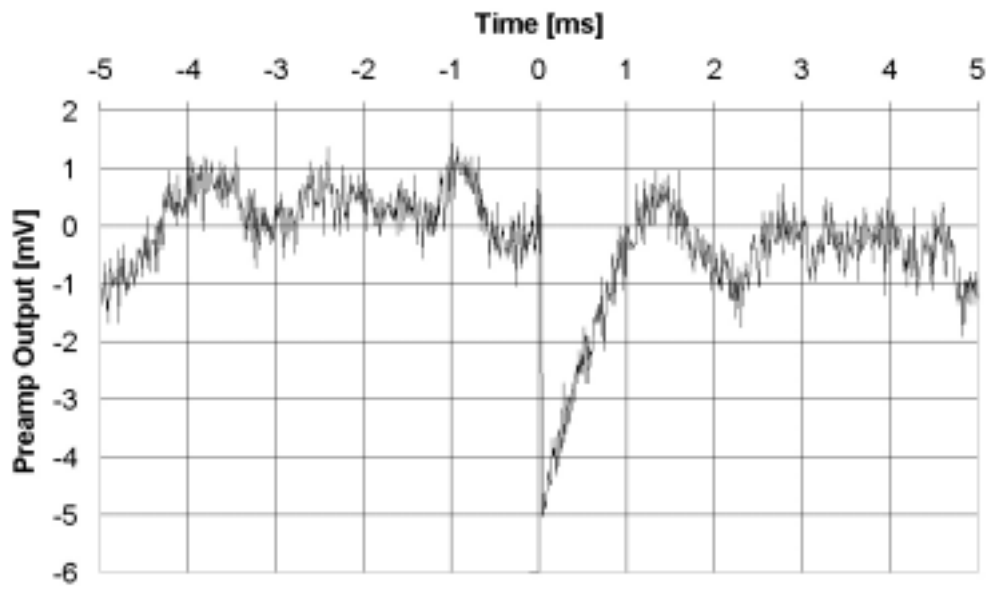


Figure 3.8: Pulse shape measured with the source.

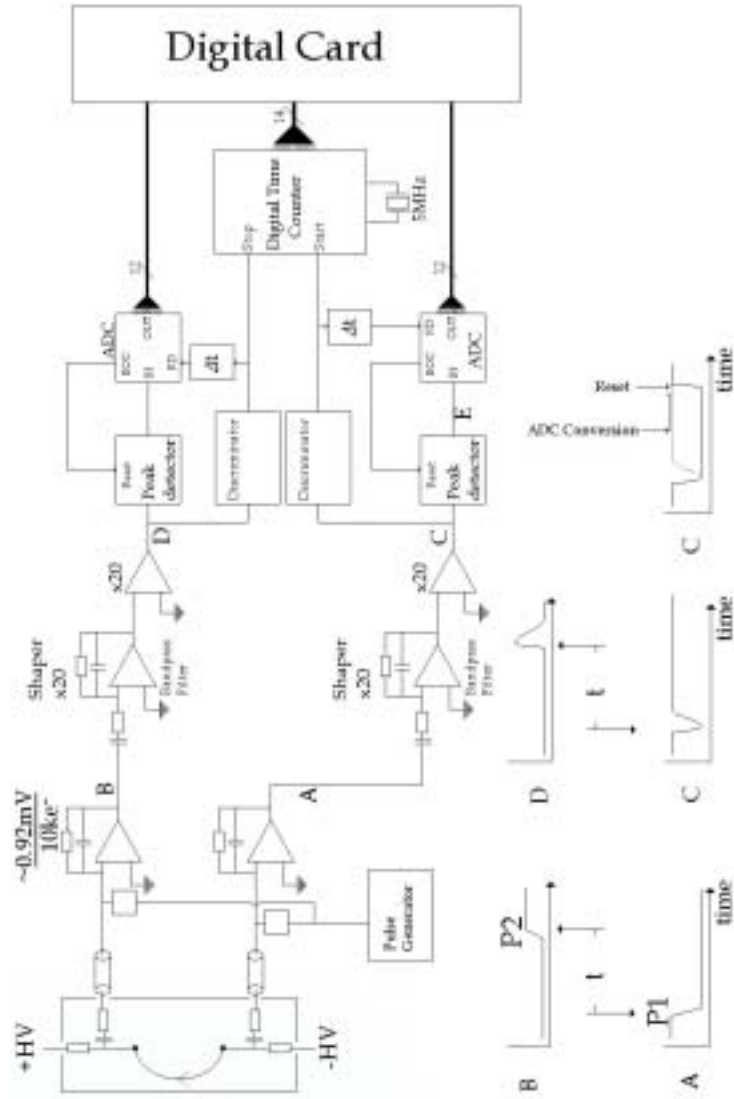


Figure 3.9: Proposed electronics for an electron life-time measurement.

The next step would be an electron life-time measurement. This requires a measurement of the pulses from the cathode (see chapter 4) and the anode and the time between the two pulses. A draft of the electronics for this measurement is shown in figure 3.9 without further comment.

Chapter 4

Measurements

In section 4.1 the calibration measurements of the electronics are presented. As a result the output voltage of the preamplifier as a function of the charge injected on the cathode is obtained. In section 4.2 the measurements of the ionization electron charge produced by the 3.72 MeV α -particles in LAr are presented. Two sources have been measured, with diameters of 0.5mm and 1.3mm respectively, and both with the HV at the anode varying between +1kV and +4kV.

4.1 Calibration of the Charge Preamplifier

The calibration measurements were made with the setup shown in figure 4.1. A rectangular pulse of 250ns width and variable pulse height from a pulse generator (type PM 5139 Fluke/Philips) was sent through a voltage divider to the cathode. The charge injected is given by:

$$Q = I \cdot \Delta t \quad (4.1)$$

where Δt is the pulse width and I is the current generated by the rectangular pulse through the attenuator, i.e.

$$I \simeq \frac{V_p R_4 R_6}{R_7 (R_5 + R_6) (R_4 + 50\Omega)} \quad (4.2)$$

here $R_5 + R_6 \gg R_4$; V_p is the output voltage of the pulse generator and the 50Ω is its internal resistance. With the resistor values of figure 4.1 we find:

$$Q \simeq 1.27 \cdot 10^{-15} \frac{C}{V} \cdot V_p \quad (4.3)$$

equivalent to

$$N \simeq 7940 \frac{\#e^-}{V} \cdot V_p \quad (4.4)$$

where N is the number of electrons injected.

The measured pulse height spectra of output voltages for four different charges injected are shown in figure 4.2. In figure 4.3 the mean values of the four spectra are plotted as a function of the injected charge. The slope of the fitted straight line gives the sensitivity of $\frac{0.92mV}{10^4e^-}$.

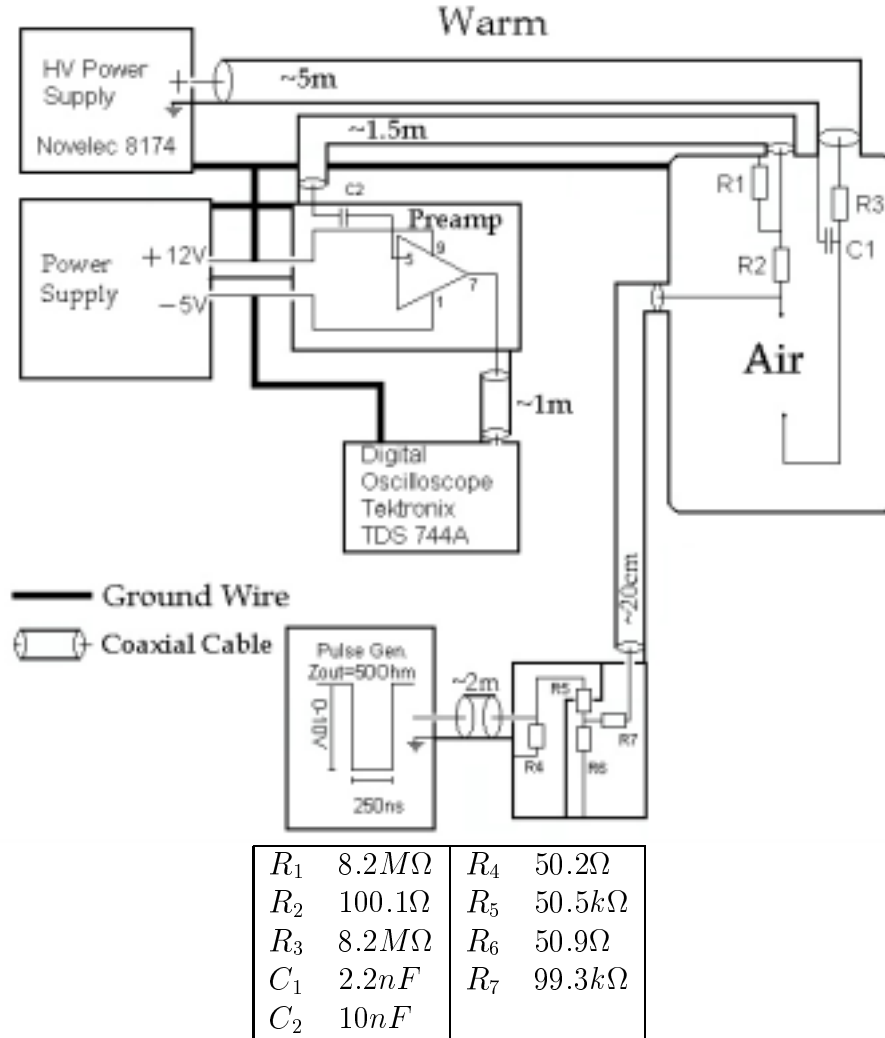


Figure 4.1: Electronics scheme for the calibration measurements.

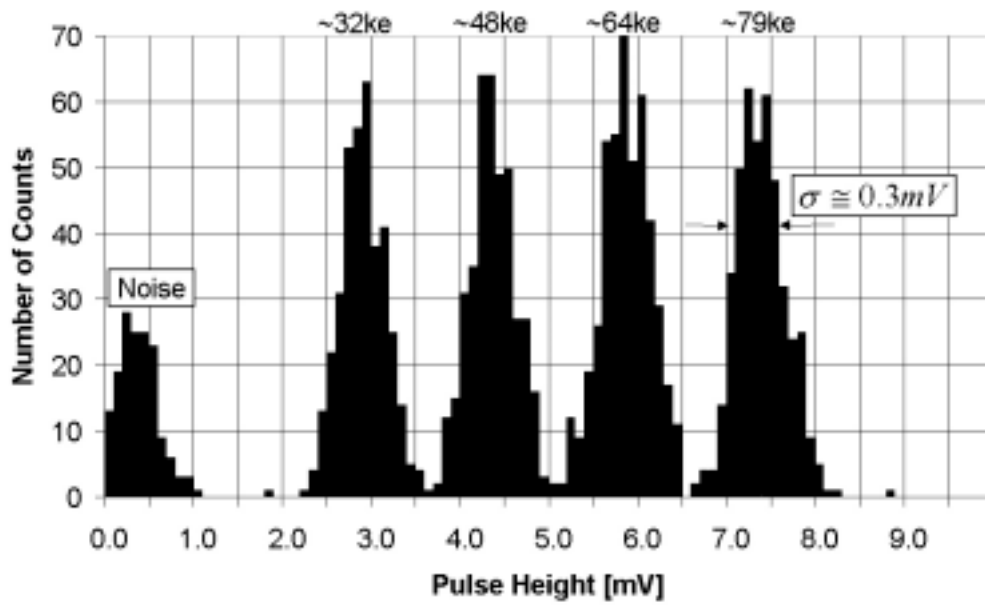


Figure 4.2: Pulse height spectra measured for different charges injected from a pulse generator on the cathode.

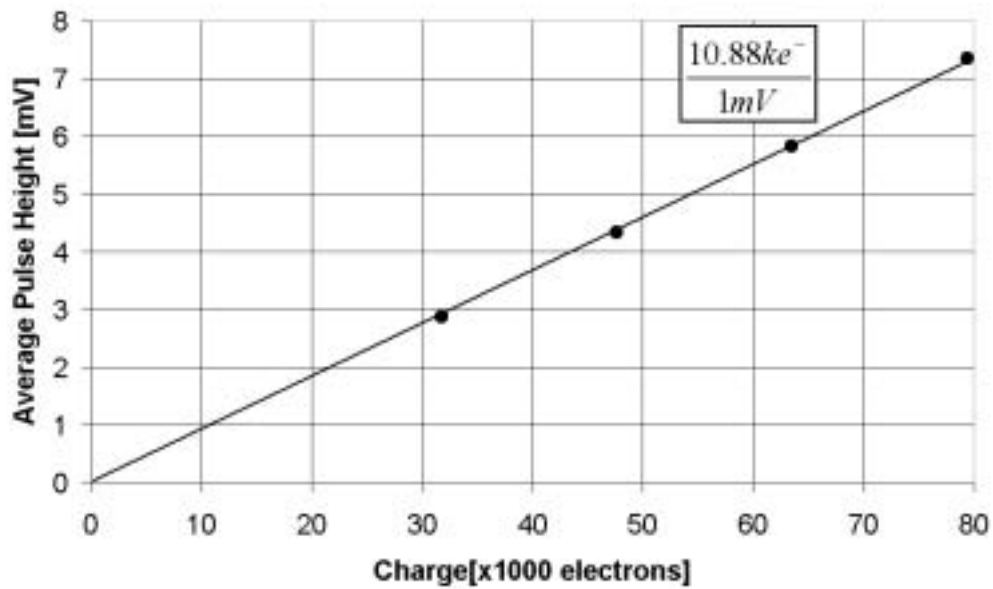


Figure 4.3: Calibration of the preamplifier: output voltage as a function of the charge input. The dots are the average pulse heights of the four spectra shown in figure 4.2.

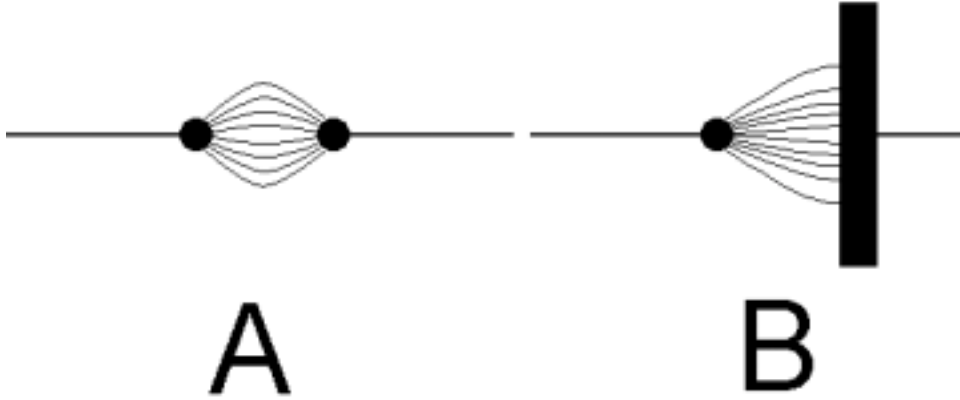


Figure 4.4: The two electrode configurations used for the measurements. The distance of the electrodes is in both cases 10mm. A: Two spheres with a diameter of 0.5mm. B: A sphere with a diameter of 1.3mm and a plate with a diameter of 4cm.

4.2 Measured Charge of the Electron Cloud

In this section the results of the measurement with two sources of 0.5mm and 1.3mm diameter are presented. The distance between the electrodes was in both cases about 10mm, but the shape of the anode was spherical for the 0.5mm source (case (A) in figure 4.4), and for the 1.3mm source it was a plate with a radius of 2cm (case (B) in figure 4.4). In both cases the anode was set to $+HV$ and the cathode was on virtual ground. This means that the field generated in case (A) is equivalent to a dipole field of $+\frac{1}{2}HV$ and $-\frac{1}{2}HV$, and for case (B) it is equivalent to a dipole field of $+HV$ and $-HV$. This difference is taken into account for the comparison of the data with the simulation.

Despite the effort spent to cover the LAr against the air, the impurity of the LAr was increasing with time, resulting in a reduction of the measured pulse heights. This is seen in figure 4.5, showing a scatter plot of measured pulse height spectra versus the time elapsed after a new LAr filling of the dewar. For the measurements shown in figure 4.5 a stainless steel dewar was used. This dewar exchanged for the subsequent measurements with a glass dewar, for which the pulse height reduction with time was much less. In addition, only the data taken within four hours after a new LAr filling were used for the comparison with the calculations so that the effect of a decreasing LAr purity was negligible.

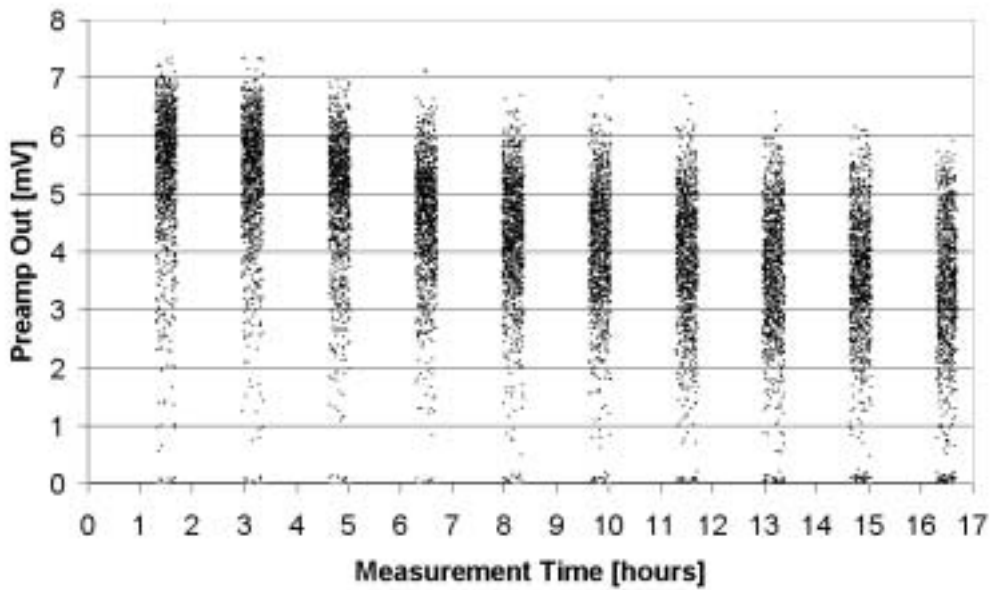


Figure 4.5: Scatter plot of the measured pulse heights as a function of the time elapsed after filling the dewar with LAr.

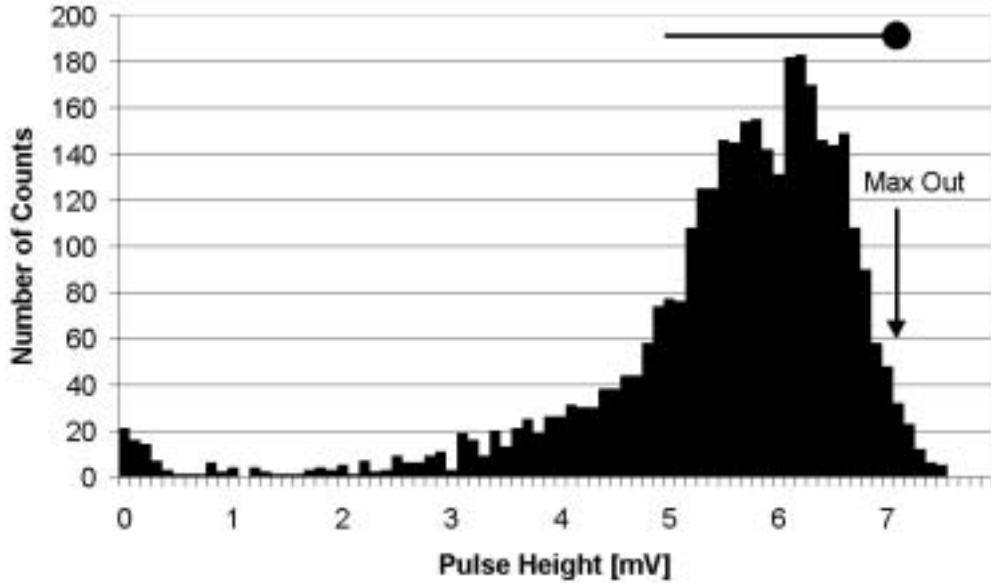


Figure 4.6: Pulse height spectrum measured with a source of 0.5mm diameter with the HV=4kV

A pulse height spectrum measured with the source of 0.5mm diameter at a HV of 4kV is shown in figure 4.6. Although the α -particles emitted from the Pb^{210} -nuclei are monoenergetic, they are emitted from the source at all angles from varying depths resulting in a broad spectrum of pulse heights with a tail towards small pulses. However, for the comparison with the calculation, only the α -particles depositing their total kinetic energy (3.72MeV) in the LAr should be considered. The pulse height corresponding to these particles is chosen as indicated by the arrow in figure 4.6. This point is about one standard deviation of the electronic resolution (0.3mV) below the end point of the spectrum. This point is also indicated as a black dot on top of the spectrum and the horizontal line is a measure of the width of the spectrum. The black dot with the straight line is used to represent the measurements in the following comparisons with the calculation.

The figures 4.7 and 4.8 show the measured number of electrons for the two sources as a function of the HV. The curves are the calculated values.

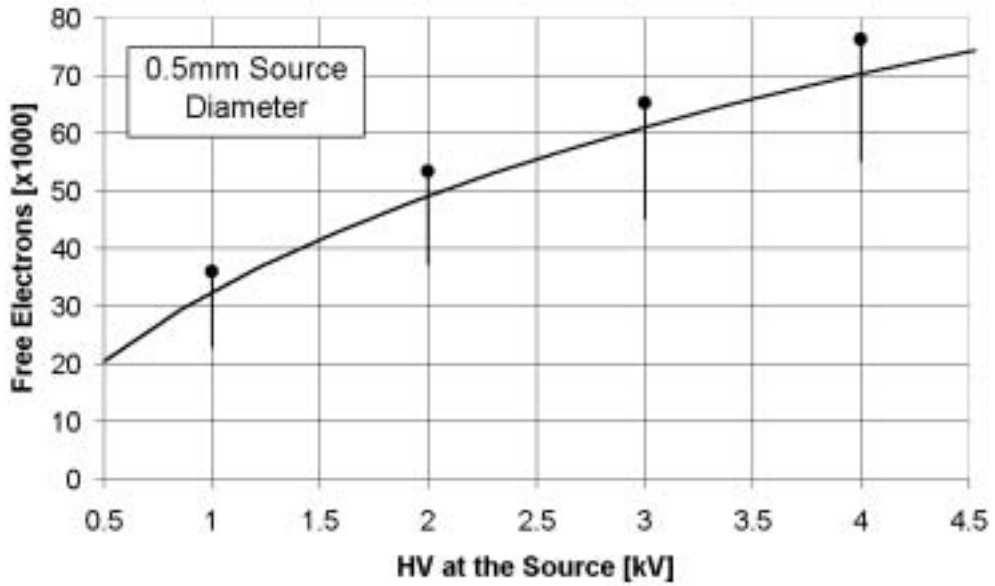


Figure 4.7: Measured number of electrons produced by an α -particle in LAr for the source diameter of 0.5mm. The curve gives the calculated values.

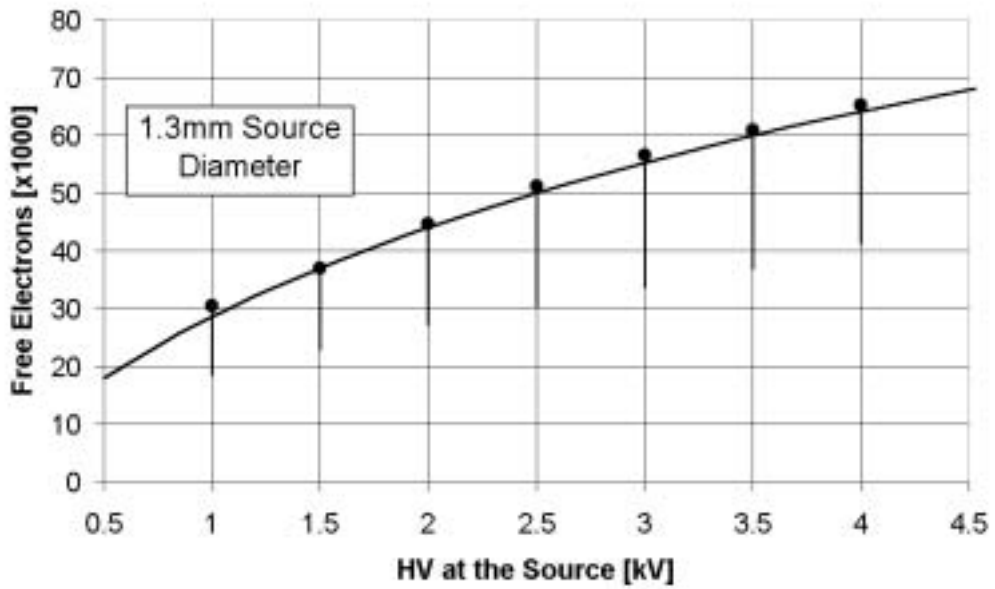


Figure 4.8: Measured number of electrons produced by an α -particle in LAr for the source diameter of 1.3mm. The curve gives the calculated values.

Chapter 5

Conclusion

This work has established, that a spherical α -source with a diameter of the order of 1mm, to which a high voltage of few kV is applied, guarantees ionization electron signals in LAr, which are much less quenched than using planar α -sources. Measurements of the number of electrons remaining after the quenching are presented in chapter 4 (see figure 4.7 and 4.8) and they agree well with the calculated values obtained from the quenching models. The program developed for the calculation of such electrons signals were necessary to design the source, which is not commercialy available. The method used to put the Pb^{210} -radionuclei on a spherical platinum support has been illustrated in section 3.2.

The two spherical electrodes (one of them is the source) generate a dipole E-field, which is optimized to limit the recombination of electron-ion pairs produced by the α -particles and, at the same time, to produce a low E-field in the central drift region for long drift times. With this configuration it is possible to reach about 200kV/cm on the surface of the source and to have less than 1V/cm over a wide drift region. In addition, the high E-field near the source has the advantage, that the free electrons are fast moving away from the source, which generates a well triggerable signal.

Drift time calculations with a dipole field show that measurements of mean life-times of the order of a few ms are easily achievable. These calculations have given important information for the design of the purity monitor.

Together with the mechanical construction of the purity monitor, also the electronics was studied to maximize the signal to noise ratio. A scheme of the electronics and the data acquisition system for a future measurement of the electron life-time has also been presented.

It remains to measure the signal of the electron cloud at the end of the drift, i.e. the signal coming form the anode, and thus be able to measure the drift time.

Bibliography

- [1] ICANOE proposal, CERN/SPSC 99-25 (1999)
- [2] M.Adams et al., ATLAS Internal Note, ATLAS-LARG-NO-053, CERN 1996
- [3] The European Physical Journal C, p.144 (1998)
- [4] J.Thomas and K.A.Imel, Phys. Rev. A **36**, 614 (1987)
- [5] A.M. Kalinin et al., ATLAS Internal Note, ATLAS-LARG-NO-058, CERN 1996
- [6] Handbook of Chemistry and Physics, 60th Edition (1980)
- [7] Table of Isotopes, 7th Edition (1978), p.1349
- [8] Private communication Prof. B. Eichler, Radiochemistry Department, PSI, CH-5232 Villigen, Switzerland.
- [9] Dehoplast RCH 1000 (Low Pressure Polyethylene)
- [10] Private communication P. Cennini, CERN, July 2000